

# Time-Reversal Symmetry-Breaking Nematic Insulators near Quantum Spin Hall Phase Transitions

Fei Xue<sup>1,\*</sup> and A.H. MacDonald<sup>1,†</sup>

<sup>1</sup>*Department of Physics, University of Texas at Austin, Austin TX 78712*

(Dated: February 16, 2022)

We study the phase diagram of a model quantum spin Hall system as a function of band inversion and band-coupling strength, demonstrating that when band hybridization is weak, an interaction-induced nematic insulator state emerges over a wide range of band inversion. This property is a consequence of the long-range Coulomb interaction, which favors interband phase coherence that is weakly dependent on momentum and therefore frustrated by the single-particle Hamiltonian at the band inversion point. For weak band hybridization, interactions convert the continuous gap closing topological phase transition at inversion into a pair of continuous phase transitions bounding a state with broken time-reversal and rotational symmetries. At intermediate band hybridization, the topological phase transition proceeds instead via a quantum anomalous Hall insulator state, whereas at strong hybridization interactions play no role. We comment on the implications of our findings for InAs/GaSb and HgTe/CdTe quantum spin Hall systems.

PACS numbers: 71.35.Lk, 73.21.Fg

*Introduction.*— The quantum spin Hall insulator (QSHI) is a state of two-dimensional matter that supports gapless helical edge modes protected by time-reversal symmetry[1–4]. Recent experiments in high-quality HgTe/CdTe[5–9] and type-II InAs/GaSb[10–14] quantum wells (QWs) have demonstrated that phase transitions between normal insulators and QSHIs can be generated in QW systems by engineering a band crossing between conduction and heavy-hole bands. In this Letter we show that when band hybridization at finite momenta is weak, electron-electron interactions can alter the character of these transition by inserting an intermediate gapped electron nematic insulator state between the normal insulator and QSHI states(NI/QSHI). Our principle results are summarized in Fig. 1 in which we distinguish five phases, including a normal insulator with a full valence band and an empty conduction band, a QSHI with inverted bands at  $\vec{k} = 0$  and an avoided crossing gap at finite momentum, a nematic insulator state in which both rotational symmetry and time-reversal symmetry are broken, an XY insulator, and a quantum anomalous Hall insulator(QAHI). We explain why the nematic state is made inevitable by the large energy difference between  $s$ -wave and  $p$ -wave Wannier excitons in two dimensions, and by the tendency of dilute excitons with repulsive interactions to condense[15–17].

Although our conclusions are quite general, the detailed calculations described below employ a four-band Bernevig-Hughes-Zhang (BHZ) model[3, 4], which describes inversion between quantum well  $s$  and heavy-hole states. We neglect bulk inversion asymmetry and structural inversion asymmetry terms in the band Hamiltonian because they are normally small[18]. With this approximation the BHZ model separates into time-reversed diagonal blocks. In the basis  $\{|E_1 \uparrow\rangle, |H_1 \uparrow\rangle, |E_1 \downarrow\rangle, |H_1 \downarrow\rangle\}$ , the QW band Hamilto-

nian is

$$\hat{H} = \sum_{\vec{k}} \psi_{\vec{k}}^\dagger \begin{pmatrix} H_{0,\uparrow} & 0 \\ 0 & H_{0,\downarrow} \end{pmatrix} \psi_{\vec{k}} + \hat{H}_I, \quad (1)$$

where the down spin single-particle term is

$$H_{0,\downarrow} = \begin{pmatrix} \frac{\hbar^2 k^2}{2m_e} + E_c & -Ak_- \\ -Ak_+ & -\frac{\hbar^2 k^2}{2m_h} + E_v \end{pmatrix}, \quad (2)$$

where  $k_\pm = k_x \pm ik_y$ ,  $A$  is the band hybridization strength, and  $m_{e(h)}$  is the electron(hole) effective mass. Our study is motivated by recent experimental[12, 19] and theoretical[20, 21] work that has demonstrated that interactions can play an essential role near NI/QSHI phase transitions. The Coulombic electron-electron interaction Hamiltonian is

$$\hat{H}_I = \frac{1}{2S} \sum_{\sigma\sigma', s's'} \sum_{\vec{k}, \vec{k}', \vec{q}} V^{ss'}(\vec{q}) a_{\sigma s \vec{k}}^\dagger a_{\sigma' s' \vec{k}'}^\dagger a_{\sigma' s' \vec{k}'+\vec{q}} a_{\sigma s \vec{k}-\vec{q}} \quad (3)$$

where  $S$  is the two-dimensional system area,  $s(s') = c$  (conduction) or  $v$  (valence) and  $\sigma(\sigma') = \uparrow$  or  $\downarrow$  distinguish band and spin states,  $a_{\sigma s \vec{k}}^\dagger$  and  $a_{\sigma s \vec{k}}$  are creation and annihilation operators,  $V^{cc}(\vec{q}) = V^{vv}(\vec{q}) = V(\vec{q}) = 2\pi e^2/(\epsilon q)$ ,  $V^{cv}(\vec{q}) = V^{vc}(\vec{q}) = U(\vec{q}) = V(\vec{q})e^{-qd}$ , and  $d$  is the spatial separation between conduction and valence band layers. We are interested in the properties of this interacting electron system as the band gap  $E_g = E_c - E_v$  closes and changes sign.

When  $A$  vanishes, the model reduces to that of the well-understood two-dimensional excitonic insulator problem[22–30], which features a continuous phase transition between a trivial band insulator and a state that is still insulating but populated by a condensate of excitons with weakly repulsive interactions. The phase transition occurs not at  $E_g = 0$ , but at a positive  $E_g$  value

equal to the exciton binding energy. The characteristic length scale of the excitonic insulator problem is the effective Bohr radius  $a_B^* = \epsilon \hbar^2 / (m_e^2)$ , and the characteristic energy scale is the effective Rydberg  $Ry^* = e^2 / (2\epsilon a_B^*)$ . [Here,  $m = m_e m_h / (m_e + m_h)$  is the excitonic reduced mass.] We explain below how excitonic insulator physics evolves with increasing  $A / (Ry^* a_B^*)$  into a renormalized version of a single-particle NI/QSHI phase-transition physics, and why the crossover as  $A$  is varied involves

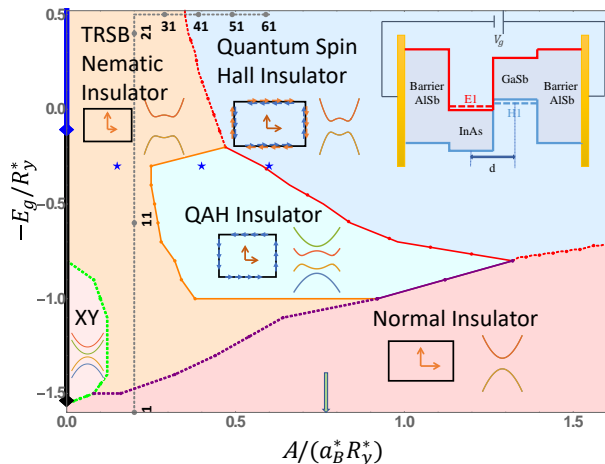


FIG. 1: (Color online) Mean-field phase diagram of a model quantum spin Hall insulator (QSHI) as a function of the band inversion parameter  $E_g$  and the band hybridization parameter  $A$ . The black diamond on the  $A = 0$  axis separates a normal insulator and an excitonic insulator (bold black), and the blue diamond marks the first-order Mott transition between an excitonic insulator and a metallic state (bold blue) that occurs at large exciton density. The exciton condensate state is characterized by spontaneous phase coherence between conduction and valence bands, and therefore exists only along the  $A = 0$  line. The stability regions of the five finite  $A$  states we have identified are distinguished by color [blue for the QSHI, cyan for the quantum anomalous Hall insulator(QAHI), orange for the time-reversal symmetry-breaking(TRSB) nematic insulator, pink for the TRSB nematic insulator state with an additional XY broken symmetry, and red for the normal insulator state]. Each state is distinguished by its typical dressed band structure, and by the presence or absence of edge states which is indicated using schematic Hall bars. Solid lines indicate first-order phase transitions and dashed lines indicate continuous phase transitions. The gray dashed line is the path connecting the normal insulator and QSHI state via the TRSB nematic insulator state discussed in the main text and illustrated in Fig. 2, and the gray circles correspond to every tenth point plotted in that figure. The blue stars specify the phase diagram points at which we illustrate quasiparticle band topological properties in Fig. 3. The inset shows a schematic band diagram for the AISb/InAs/GaSb/AISb QW system, to which the model corresponds most closely. The arrow along the horizontal axis indicates the value of the dimensionless band hybridization parameter for the case of adjacent InAs and GaSb layers.

a state with broken rotational and time-reversal symmetry. Some aspects of the physics are best illustrated using a simplified two-band model, whose properties are discussed in detail in the Supplemental Material.

*Microscopic mean-field theory.*— We first describe the results of a mean-field theory calculation that allows for all possible broken symmetries that preserve translational invariance, and then discuss how neglected quantum fluctuations might alter the resulting phase diagram. The Hartree-Fock mean-field Hamiltonian for the BHZ model is

$$\hat{H}_{MF} = \sum_{\vec{k}} \psi_{\vec{k}}^\dagger (H_0 + H_{Hartree} + H_{Fock}) \psi_{\vec{k}} \quad (4)$$

where

$$H_{Fock} = \begin{pmatrix} \Delta_{\uparrow\uparrow}^{cc}(\vec{k}) & \Delta_{\uparrow\uparrow}^{cv}(\vec{k}) & \Delta_{\uparrow\downarrow}^{cc}(\vec{k}) & \Delta_{\uparrow\downarrow}^{cv}(\vec{k}) \\ \Delta_{\uparrow\uparrow}^{vc}(\vec{k}) & \Delta_{\uparrow\uparrow}^{vv}(\vec{k}) & \Delta_{\uparrow\downarrow}^{vc}(\vec{k}) & \Delta_{\uparrow\downarrow}^{vv}(\vec{k}) \\ \Delta_{\downarrow\uparrow}^{cc}(\vec{k}) & \Delta_{\downarrow\uparrow}^{cv}(\vec{k}) & \Delta_{\downarrow\downarrow}^{cc}(\vec{k}) & \Delta_{\downarrow\downarrow}^{cv}(\vec{k}) \\ \Delta_{\downarrow\uparrow}^{vc}(\vec{k}) & \Delta_{\downarrow\uparrow}^{vv}(\vec{k}) & \Delta_{\downarrow\downarrow}^{vc}(\vec{k}) & \Delta_{\downarrow\downarrow}^{vv}(\vec{k}) \end{pmatrix}, \quad (5)$$

$$H_0 + H_{Hartree} = \zeta_{\vec{k}} s_0 \tau_0 + \epsilon_{\vec{k}} s_0 \tau_z + A k_x s_z \tau_x - A k_y s_0 \tau_y, \quad (6)$$

and  $s_i$  and  $\tau_i$  are spin and electron-hole Pauli matrices respectively. In Eq. 6  $\zeta_{\vec{k}} = \hbar^2 k^2 [1/(4m_e) - 1/(4m_h)]$  accounts for the mass difference between conduction and valence bands, which plays a minor role and is dropped below. The band-splitting term,  $\epsilon_{\vec{k}} = \hbar^2 k^2 / 4m + E_g / 2 + 2\pi e^2 n_{ex} d$ , includes an electrostatic Hartree contribution which is linear in  $d$ . In Eq. 5

$$\Delta_{\sigma\sigma'}^{ss'}(\vec{k}) = -\frac{1}{S} \sum_{\vec{k}'} V^{ss'}(\vec{k} - \vec{k}') \rho_{\sigma\sigma'}^{ss'}(\vec{k}'), \quad (7)$$

where the density matrix,

$$\rho_{\sigma\sigma'}^{ss'}(\vec{k}) = \langle a_{\sigma's'\vec{k}}^\dagger a_{\sigma s \vec{k}} \rangle - \delta_{ss'} \delta_{\sigma\sigma'} \delta_{\sigma=v}, \quad (8)$$

is defined relative to the fully filled valence band because the bare bands are assumed to be those of the normal insulator. The exciton density appearing in the Hartree term is

$$n_{ex} = \frac{1}{S} \sum_{\sigma, \vec{k}} \rho_{\sigma\sigma}^{cc}(\vec{k}). \quad (9)$$

In much of the phase diagram Eq. 4 has multiple metastable solutions. We select the mean-field ground state by computing the total energy per area:

$$\epsilon = \frac{1}{2S} \sum_{\vec{k}} Tr \{ \rho(\vec{k}) [H_0(\vec{k}) + H_{MF}(\vec{k})] \}. \quad (10)$$

The BHZ single-particle Hamiltonian  $H_0$  is isotropic and has time-reversal symmetry. Its coupling between

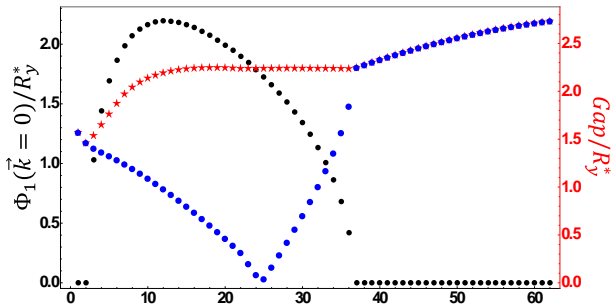


FIG. 2: (Color online) Time-reversal symmetry-breaking order parameters  $\Phi_1$  (black dots, left axis) and quasiparticle gaps (red stars, right axis) along the gray dashed line in Fig. 1, which passes through the TRSB nematic insulator state. For comparison, the blue squares show the quasiparticle gaps in the time-reversal symmetry-preserving nematic insulator state discussed in the main text, which has higher energy.

the  $s$ -wave conduction and  $p$ -wave valence bands vanishes at  $\vec{k} = 0$  because of an underlying microscopic  $C4$  rotational symmetry. It follows that rotational symmetry is broken when  $\Delta_{\sigma\sigma'}^{cv}(\vec{k} = 0) \neq 0$ , allowing us to identify  $\Phi_{N_{\sigma\sigma'}} = H_{\sigma\sigma'}^{cv}(\vec{k} = 0)$  as a, possibly spin-dependent, nematic order parameter. Similarly since  $s_0\tau_0, s_0\tau_x, s_0\tau_z, s_x\tau_y, s_y\tau_y$ , and  $s_z\tau_y$  are time-reversal invariant, it follows that when time-reversal symmetry is intact the quasiparticle Hamiltonian at wave vector  $\vec{k} = 0$  must satisfy  $H_{\uparrow\uparrow}^{ss} = H_{\downarrow\downarrow}^{ss}$ ,  $H_{\uparrow\uparrow}^{ss'} = [H_{\downarrow\downarrow}^{ss'}]^*$ ,  $H_{\sigma\sigma'}^{ss'} = -H_{\sigma\sigma'}^{s's}$ , and  $H_{\sigma\sigma'}^{ss} = 0$ , where  $s \neq s'$  and  $\sigma \neq \sigma'$ . We can define four corresponding order parameters that characterize different ways in which the system can break time-reversal symmetry:  $\Phi_1 = H_{\uparrow\downarrow}^{cv}(\vec{k} = 0) + H_{\downarrow\uparrow}^{vc}(\vec{k} = 0)$ ,  $\Phi_2 = H_{\uparrow\uparrow}^{cc}(\vec{k} = 0) - H_{\downarrow\downarrow}^{cc}(\vec{k} = 0)$ ,  $\Phi_3 = Re(H_{\uparrow\uparrow}^{cv}(\vec{k} = 0)) - Re(H_{\downarrow\downarrow}^{cv}(\vec{k} = 0)) + Im(H_{\uparrow\uparrow}^{cv}(\vec{k} = 0)) + Im(H_{\downarrow\downarrow}^{cv}(\vec{k} = 0))$ , and  $\Phi_4 = H_{\uparrow\downarrow}^{cc}(\vec{k} = 0)$ .

*Phase diagram.*— The phase diagram in Fig. 1 was constructed by identifying the lowest energy solution of Eq. 4 over a range of  $A$  and  $E_g$  values[10, 12, 31], fixing other model parameters at values appropriate for InAs/GaSb QWs: electron-hole layer separation  $d = 0.3a_B^* \sim 100\text{\AA}$ ,  $m_e = 0.023m_0$ ,  $m_h = 0.4m_0$ , and  $\epsilon \sim 15\epsilon_0$ [32, 33]. ( $a_B^* \sim 365\text{\AA}$  and  $Ry^* \sim 1.3meV$ .) In InAs/GaSb systems, the energy gap  $E_g$  can be varied by changing quantum well widths, and tuned *in situ* with external gates[10, 12]. The band hybridization parameter  $A$  can be varied by inserting AlSb barrier layers between the InAs electron layer and the GaSb hole layer[31].

The black diamond on the vertical axis ( $A = 0$  line) in Fig. 1 marks the point at which the band gap is reduced to the spatially indirect exciton binding energy. The  $s$ -wave exciton condensate state[22, 30] which forms at this point when  $A = 0$  establishes spontaneous co-

herence between bands that is peaked at  $\vec{k} = 0$ , is independent of momentum orientation  $\theta_k$ , and has an energy that is invariant under independent spin reorientations in either layer. We find that at finite  $A$  the ground state prefers that coherence be established between opposite spins, and that the two independent opposite-spin coherence parameters  $H_{\uparrow\downarrow}^{cv}(\vec{k} = 0)$  and  $H_{\downarrow\uparrow}^{vc}(\vec{k} = 0)$  prefer to have the same sign, breaking rotational and time-reversal symmetry. This arrangement minimizes the frustration between  $s$ -wave exciton condensation and single-particle interband coupling that is proportional to  $\exp(i\theta_k)$  and diagonal in spin. The occupied quasiparticles have band-spin spinors of the form  $(u_{\vec{k}}, v_{\vec{k}}e^{-i\theta_{\vec{k}}}, u_{\vec{k}}e^{-i\theta_{\vec{k}}}, v_{\vec{k}})^T$  allowing their projection onto a definite spin to have  $p$ -wave interband coherence, while retaining opposite spin coherence that is independent of  $\theta_k$ . Interband coherence at  $\vec{k} = 0$  breaks the BHZ model's rotational symmetries. In the simplified spinless two-band model (see supplemental material), the frustration between  $s$ -wave excitons and  $p$ -wave contributions to the band Hamiltonian is resolved in momentum space by moving the vortex in  $H^{cv}$  away from  $\vec{k} = 0$ . Adding the spin degree of freedom enables a resolution of the frustration between interaction and band terms in the Hamiltonian that is simpler and more elegant than in the spinless case discussed in the Supplementary Material.

We do find solutions of the mean-field equations with  $H_{\uparrow\downarrow}^{cv}(\vec{k} = 0) = -H_{\downarrow\uparrow}^{vc}(\vec{k} = 0)$ , preserving time-reversal symmetry, but these always have higher total energy than the time-reversal symmetry-breaking (TRSB)  $\Phi_1 \neq 0$  solutions. TRSB states are energetically preferred because they provide a continuous phase transition path between ordinary insulator states and QSHI states along which the gap is not required to vanish [4, 21, 34]. The quasiparticle Hamiltonian of the time-reversal symmetry-preserving nematic state has the form  $\xi_{\vec{k}}s_0\tau_z + Ak_x s_z \tau_x - Ak_y s_0 \tau_y + X s_y \tau_y$ , where  $X$  is an exchange energy, and therefore a gap  $2\sqrt{\xi_{\vec{k}}^2 + (Ak_y - X)^2}$  that vanishes when  $\xi_{\vec{k}} = 0$  and  $Ak_y = X$ . These conditions are satisfied along a line in phase space that cannot be avoided in transiting between normal and QSHI states, as illustrated by the gap closing phase transition (blue squares) in Fig. 2. On the other hand, the TRSB state has a mean-field Hamiltonian of the form  $\xi_{\vec{k}}s_0\tau_z + Ak_x s_z \tau_x - Ak_y s_0 \tau_y + X s_x \tau_x$ , implying a gap,  $2\sqrt{\xi_{\vec{k}}^2 + (Ak)^2 + X^2}$ , that needs not to vanish.

Fig. 1 identifies five distinct phases with different order parameters and band topologies. In addition to the normal and QSHI phases of the bare bands, three interaction-induced phases appear all of which break time-reversal symmetry. The TRSB nematic insulator has nonzero values for  $\Phi_N$  and  $\Phi_1$ ; the  $XY$  insulator has spontaneous transverse spin polarization in addition so that  $\Phi_N$ ,  $\Phi_1$ , and  $\Phi_4$  are all non-zero; the QAHI state has a nonzero value of order parameter

$\Phi_2$ , but is not nematic. Its presence close to the line along which the interaction renormalized band gap vanishes is closely related to the heavily studied instabilities of massless[35, 36] two-dimensional Dirac models at strong interactions. [ $A/(Ry^*a_B^*) = 2[e^2/(\hbar v\epsilon)]^{-1}$  where  $v = A/\hbar$  is the band velocity at  $\xi_{\vec{k}=0} = 0$ .] The normal insulator and the QSHI preserve time-reversal and rotational symmetry, and differ only in the sign of the renormalized band gap at  $\vec{k} = 0$ .

At large values of  $A$  the NI/QSHI transition is not altered by interactions. At intermediate values of  $A$ , we find that the NI/QSHI transition proceeds via an intermediate QAHI state that is separated from both NI and QSHI states by first-order phase transitions, similar to the behavior predicted by dynamic mean-field theory for Hubbard model systems[37] and by mean-field theory for interacting Kane-Mele Hubbard models[38]. The QAHI phase is characterized by a  $Us_z\tau_z$  mean-field term and has a  $\Phi_2$  TRSB order parameter. To characterize the topological properties of the various different phases we perform a continuum model version of a Wilson loop[39, 40] calculation for the two occupied bands. We evaluate the non-Abelian  $2 \times 2$  Berry connection matrix  $F_{i,i+1}^{m,n} = \langle u_i^m | u_{i+1}^n \rangle$  along square loops of different perimeters surrounding the momentum space origin. Then we construct a matrix  $D$  by finding the product of all  $F$ s along the square path labeled by  $k$ , equal to half of the square's edge. These matrices have two eigenvalues and phase angles  $\theta_k$ . The change in the sum of the  $\theta_k$  values between  $k = 0$  and a finite value of  $k$  is[39, 40] equal to the integral of the momentum space Berry curvature over the enclosed area. Because band inversion occurs only near  $k = 0$ , we can identify the topological properties of quasiparticle bands from these small  $k$  continuum model calculations.

In Fig. 3 we plot typical  $\theta$  profiles for TRSB nematic insulator, QAHI, and QSHI phases. Fig. 3(a) shows that the TRSB nematic insulator is topologically trivial, with two winding number zero bands. The  $\theta_k$  profiles of the XY insulator, and normal insulator states (not shown) are similar to those of the TRSB nematic insulator state. Fig. 3(b) shows that the QAHI state is topologically non-trivial with one band winding the cylinder once, corresponding to total Chern number equal to 1. Similarly Fig. 3(c) demonstrates the topological nontrivial  $Z_2 = 1$  behavior expected for a QSHI, with two bands winding the cylinder once in opposite directions. The topology can be identified from these Chern number calculations because up and down spin sectors are decoupled.

*Discussion.*— The BHZ model applies to HgTe/CdTe and InAs/GaSb quantum well systems. In the former case the electron and hole bands are strongly coupled because they both reside in HgTe. The dimensionless band-coupling parameter  $A/(Ry^*a_B^*)$  is therefore large[18] and interactions are unimportant. The phase diagram in Fig. 1 can be fully explored experimentally in InAs/GaSb

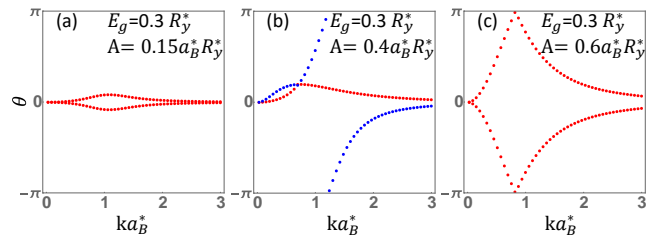


FIG. 3: (Color online) Phase angle  $\theta$  profiles at the three different phase diagram points marked in Fig. 1. For the left (TRSB nematic insulator) and right (QSHI) states the quasi-particle bands are doubly degenerate. In the middle panel (QAHI state) the blue and red dots distinguish the phase angles of the two occupied bands. (a) TRSB nematic insulator state with topologically trivial bands, (b) QAHI with one nonzero Chern number band, and (c) QSHI with two opposite nonzero Chern number bands.

systems by inserting AlSb layers between the InAs and GaSb to vary  $A$ . Indeed important progress has already been achieved in recent studies of the no AlSb[12] and thick AlSb[31] ( $A = 0$ ) limits. In the absence of AlSb, it was shown[12] that the band gaps in the QSHI state are larger than expected on the basis of single-particle physics alone, as predicted by our mean-field calculations, and that they survive in-plane magnetic fields that are expected to suppress single-particle contributions. Qualitatively, in-plane magnetic fields have an effect similar to reducing  $A$ . The observation that the gap does not vanish even as its single-particle support is removed is consistent with our findings. Further work will be necessary to determine whether or not the resulting state has the broken time-reversal and rotational symmetry that we expect in the small  $A$  limit.

It is important to recognize that mean-field theory can err both quantitatively and qualitatively. For example, the stability region of the QAHI state along the  $\xi_{\vec{k}=0} = 0$  line is expected[35, 36] to be shifted toward stronger interactions (smaller  $A$ ) by quantum fluctuations, and could potentially be preempted by the TRSB nematic insulator state.

The presence of a QAHI state can be established experimentally by performing nonlocal transport measurements, similar to those[5, 10] used to establish the QSHI state to establish that edge states have chiral rather than helical character. The appearance of an exciton condensate state along the  $A = 0$  line, where the physics is simplified by binding of electrons and holes into bosonic excitons, is certain, but the density at which the Mott transition occurs[41–44] is difficult to estimate accurately. Since it can be viewed as an exciton condensate that is weakly perturbed by band hybridization, the appearance of a TRSB nematic insulator state is also certain, but its persistence in the upper left-hand side of our phase diagram (Fig. 1) where it competes with paramagnetic

metallic states is uncertain. The presence of a TRSB nematic insulator state can be established by performing counterflow experiments[45] and by demonstrating the absence of edge states. (A similar nematic phase has been proposed in the vicinity of quantum anomalous Hall states[46, 47].) Very recent experimental studies[31] have demonstrated that a gapped state, presumably the exciton condensate, is still present at  $n_{ex}a_B^{*2} \approx 0.03$ . These findings suggest that the full region of the phase diagram in Fig. 1 is open to experimental study. Recently, a new type of QSHI has been discovered experimentally[48–50], which is described by band models[51] that are distinguished from the BHZ model studied here mainly by large anisotropies and also subject to interaction-induced broken symmetries.

This work was primarily supported by the U.S. Department of Energy, Office of Science, Basic Energy Sciences under Award No. DE-FG02-ER45958 and by the Welch Foundation under Grant No. TBF1473.

### Supplemental Material

In this supplemental material, we will discuss a simple one-spin two-band case on interaction-induced nematic insulators near quantum spin Hall phase transitions. The single particle Hamiltonian for down spin in BHZ model is:

$$H_{0,\downarrow} = \begin{pmatrix} \frac{\hbar^2 k^2}{2m_e} + E_c & -Ak_- \\ -Ak_+ & -\frac{\hbar^2 k^2}{2m_h} + E_v \end{pmatrix}, \quad (11)$$

where  $k_{\pm} = k_x \pm ik_y$ ,  $A$  is the band coupling strength,  $m_{e(h)}$  is the electron(hole) effective mass.

The Coulombic electron-electron interaction Hamiltonian

$$\hat{H}_I = \frac{1}{2S} \sum_{ss'} \sum_{\vec{k}, \vec{k}', \vec{q}} V^{ss'}(\vec{q}) a_{s\vec{k}}^{\dagger} a_{s'\vec{k}'}^{\dagger} a_{s'\vec{k}'+\vec{q}} a_{s\vec{k}-\vec{q}} \quad (12)$$

where  $S$  is the two dimensional system area, conduction or valence bands are labeled by  $s(s') = c$  or  $v$ ,  $a_{s\vec{k}}^{\dagger}$  and  $a_{s\vec{k}}$  are quantum well (QW) conduction(valence) band electron creation and annihilation operators,  $V^{cc}(\vec{q}) = V^{vv}(\vec{q}) = V(\vec{q}) = 2\pi e^2/(\epsilon q)$ , and  $V^{cv}(\vec{q}) = V^{vc}(\vec{q}) = U(\vec{q}) = V(\vec{q})e^{-qd}$ . We are interested in the properties of this interacting electron system as the band gap  $E_g = E_c - E_v$  closes and changes sign.

When  $A$  vanishes, the model reduces to that of the two-dimensional excitonic insulator problem,[22–30] in which electron-electron interactions play a central role. For gaps larger than the exciton binding energy, the ground state at  $A = 0$  is a trivial band insulator. For gaps slightly smaller than the exciton binding energy, there is a continuous phase transition to a ground state that is still insulating but populated by a condensate of excitons with weakly repulsive interactions. At still smaller gaps, there is a first order phase transition[41–44] to a conducting state with free electrons and holes. The characteristic

length scale of the excitonic insulator problem is the effective Bohr radius  $a_B^* = \epsilon \hbar^2/(m_e^2)$ , and the characteristic energy scale is the effective Rydberg  $Ry^* = e^2/(2\epsilon a_B^*)$ . (Here  $m = m_e m_h/(m_e + m_h)$  is the excitonic reduced mass.) When  $A$  is very much larger than  $Ry^* a_B^*$ , interactions play an unimportant role. We explain below how the excitonic insulator physics evolves with increasing  $A$  into a renormalized version of single-particle normal insulator/Quantum spin Hall insulator (NI/QSHI) phase-transition physics, and why the crossover is punctuated by a nematic state with broken rotational symmetry.

*Microscopic Mean-Field Theory:*— Because spin-orbit coupling terms that mix spins are absent in the BHZ model, we focus initially on a single block. The Hartree-Fock mean-field Hamiltonian for down spins,

$$\hat{H}_{MF} = \sum_{\vec{k}} (a_{c\vec{k}}^{\dagger}, a_{v\vec{k}}^{\dagger}) \begin{pmatrix} \zeta_{\vec{k}} + \xi_{\vec{k}} & -\Delta_{\vec{k}} \\ -\Delta_{\vec{k}}^* & \zeta_{\vec{k}} - \xi_{\vec{k}} \end{pmatrix} \begin{pmatrix} a_{c\vec{k}} \\ a_{v\vec{k}} \end{pmatrix}. \quad (13)$$

Here  $\zeta_{\vec{k}} = \hbar^2 k^2 [1/(4m_e) - 1/(4m_h)]$  accounts for the mass difference between conduction and valence bands which plays a very minor role in selecting between insulating many-particle ground states and is dropped below. The difference ( $\xi_{\vec{k}}$ ) between conduction and valence band energies and the band coupling amplitude ( $\Delta_{\vec{k}}$ ) are both renormalized by interactions and determined by solving the following self-consistent field equations:

$$\xi_{\vec{k}} = \frac{\hbar^2 k^2}{4m} + \frac{E_{gap} + 4\pi e^2 n_c d/\epsilon}{2} - \frac{1}{2S} \sum_{\vec{k}'} V(\vec{k} - \vec{k}') (1 - \xi_{\vec{k}'}/E_{\vec{k}'}), \quad (14)$$

$$\Delta_{\vec{k}} = \frac{1}{2S} \sum_{\vec{k}'} U(\vec{k} - \vec{k}') \frac{\Delta_{\vec{k}'}}{E_{\vec{k}'}} + Ak_-,$$

where  $E_{\vec{k}} = \sqrt{\xi_{\vec{k}}^2 + |\Delta_{\vec{k}}|^2}$ , and  $d$  is the vertical separation between electron and hole layers. Note that the important model Hamiltonian parameter  $E_{gap} = E_c - E_v$  is equal to the quasiparticle energy gap at  $= 0$  only when  $\Delta_{\vec{k}} = 0$  so that the conduction band is completely empty and the valence band full. In Eq. 14

$$n_c = \frac{1}{2S} \sum_{\vec{k}} (1 - \xi_{\vec{k}}/E_{\vec{k}}) \quad (15)$$

is the charge density in the conduction band layer.

$\Delta_{\vec{k}} = |\Delta_{\vec{k}}| \exp(i\phi_{\vec{k}})$  in Eq. 13 is a complex function of  $\vec{k}$ . In the  $A = 0$  excitonic insulator state  $\Delta_{\vec{k}}$  is independent of  $\theta_{\vec{k}} = \arctan(k_y/k_x)$ . In the large  $A$  limit, however,  $\Delta_{\vec{k}}$  has the same  $\theta_{\vec{k}}$ -dependence as  $Ak_- = Ak \exp(-i\theta_{\vec{k}})$ . The  $k$  and  $\theta_{\vec{k}}$  dependence at intermediate values of  $A$  minimizes the total energy per area,



$$\epsilon = \frac{1}{2S} \sum_{\vec{k}} \left[ \left( \frac{\hbar^2 k^2}{4m} + \frac{E_{gap}}{2} + \xi_{\vec{k}} \right) \left( 1 - \frac{\xi_{\vec{k}}}{E_{\vec{k}}} \right) - \frac{|\Delta_{\vec{k}}|^2 + Ak|\Delta_{\vec{k}}|\cos(\theta_{\vec{k}} + \phi_{\vec{k}})}{E_{\vec{k}}} \right]. \quad (16)$$

*Phase Diagram*—The phase diagram in Fig. 4 was constructed by solving Eqs 14 over a range of  $A$  and  $E_{gap}$  values,[10] fixing other model parameters at values appropriate for InAs/GaSb QWs: electron-hole layer separation  $d = 0.3a_B^* \sim 100\text{\AA}$ ,  $m_e = 0.023m_0$ ,  $m_h = 0.4m_0$ , and  $\epsilon \sim 15\epsilon_0$ [32, 33]. These values set  $a_B^* \sim 365\text{\AA}$  and

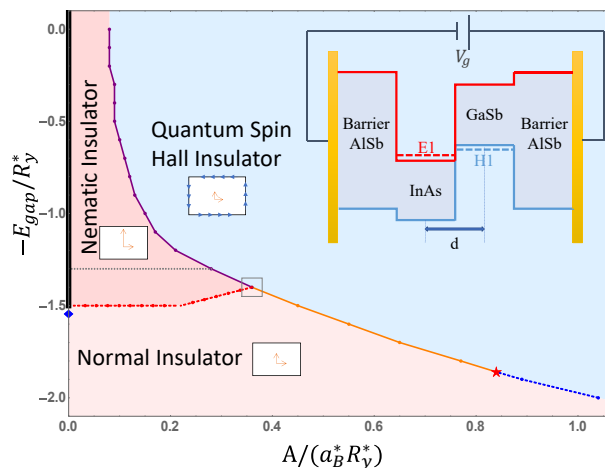


FIG. 4: (Color online) Mean-field phase diagram of a model quantum spin Hall insulator (QSHI) as a function of band inversion parameter  $E_{gap}$  and band coupling strength parameter  $A$ . The blue square on the  $A = 0$  axis separates a normal insulator state and an exciton condensate (XC) state which is present where the axis is bold. The light blue area denotes QSHI phase where edge state for one spin exists and bulk transport is isotropic. The dark pink area denotes nematic insulator phase where no edge state exists and bulk transport is anisotropic due to rotational symmetry breaking. The light pink area denotes normal insulator phase where no edge state exists and bulk transport is isotropic. The purple line describes first order phase transition boundary between nematic insulator and QSHI. The red dashed line describes second order phase transition boundary between normal insulator and nematic insulator. The orange line describes first order NI/QSHI phase transition boundary. The blue dashed line describes second order NI/QSHI phase transition boundary. Red star denotes critical value where NI/QSHI phase transition becomes continuous. The gray square denotes the parameter space where we calculate off-diagonal and diagonal terms at  $\vec{k} = 0$  in Fig. 7. The inset shows a schematic band diagram for the AlSb/InAs/GaSb/AlSb QW system to which the model corresponds most closely. In this system electron and hole layers are spatially separated and the band inversion parameter  $E_{gap}$  can be tuned by adjusting gate voltage that apply electric fields across AlSb barriers.

$Ry^* \sim 1.3meV$ . In InAs/GaSb systems, the energy gap  $E_g$  can be varied by changing quantum well widths, and tuned *in situ* with external gates. The band hybridization parameter  $A$  can be varied by inserting AlSb layers between the InAs electron layer and the GaSb hole layer.

The blue square on the vertical axis  $A = 0$  in Fig. 4 marks the point at which the band gap is reduced to the spatially indirect exciton binding energy. Our main finding is that the exciton condensate state[22, 30] which forms at this point when  $A = 0$  and induces inter-band coherence that is strongest at  $\vec{k} = 0$  and phase  $\phi_{\vec{k}}$  that is independent of momentum orientation  $\theta_{\vec{k}}$ , is only weakly perturbed by band hybridization;  $\phi_{\vec{k}}$  is independent of  $\theta_{\vec{k}}$  in the  $A = 0$  ground state because only  $s$ -wave excitons are energetically allowed at relevant  $E_g$  values. We find that the interaction contribution to  $\Delta_{\vec{k}}$  initially changes gradually with  $A$ . When the single-particle contribution is added  $|\Delta_{\vec{k}}|$  and the quasiparticle energy  $E_{\vec{k}}$  are no-longer independent of momentum orientation  $\theta_{\vec{k}}$ , inducing anisotropy in all electronic properties. Indeed, because the  $\vec{k} = 0$  electron and hole states have different angular momentum, hybridization between them that does have a constant value of  $\theta_{\vec{k}} + \phi_{\vec{k}}$  must break the BHZ model's rotational symmetries. We identify the small  $A$  state at gaps that are smaller than the exciton binding energy as a nematic insulator.

The relationship of the nematic insulator to the NI/QSHI phase transition is best addressed by considering the Chern index of the spin-projected quasiparticle bands. Because  $\Delta_{\vec{k}}$  is complex, it will vanish at isolated points in momentum space. Because the single-particle contribution dominates at large  $k$ , the line integral of its phase derivative around a large diameter circle must equal the single-particle value  $-2\pi$ . We conclude that  $\Delta_{\vec{k}}$  always has isolated vortex at some value of  $\vec{k}$ . Whenever the vortex is not at  $\vec{k} = 0$ , rotational symmetry is broken. Similarly the renormalized band gap function  $\xi_{\vec{k}}$  is real and therefore can vanish along a line, referred to below as the zero-line, in momentum space. By taking note of the different sense of dispersion in the conduction and valence bands, we see that the occupied quasiparticle band has a non-zero Chern number when the zero-line is present and, the vortex is enclosed by the zero-line. To identify vortex positions, we calculated the phase winding around each momentum mesh plaquette on our grid. Plaquettes with  $2\pi$  phase winding are shaded black in Fig. 5 and surrounded by an arrow indicating the sense of vorticity. The nematic state in Fig. 4 is distinguished

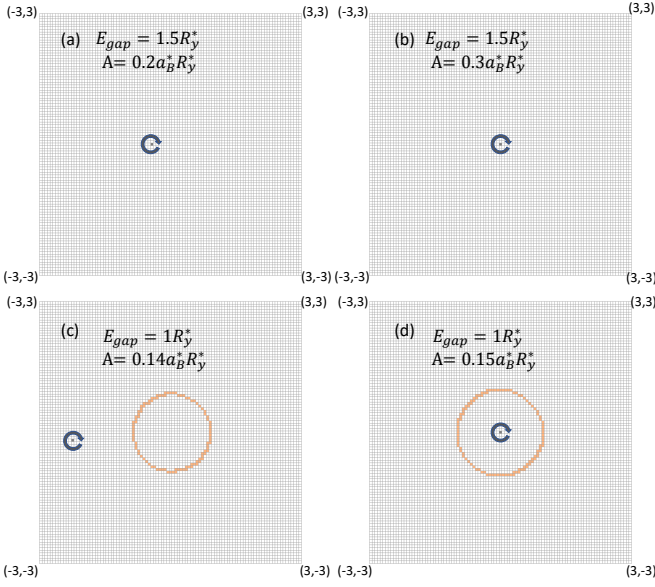


FIG. 5: (Color online) Plots of vortex points and zero-lines on the momentum grid under different circumstances where black plaquettes denote vortex points surrounded by a schematic arrow and orange plaquettes denote  $\xi_{\vec{k}} = 0$ . (a) Nematic insulator state at  $(\mu = -1.5, A = 0.2)$ ; (b) Normal insulator state at  $(\mu = -1.5, A = 0.3)$ ; (c) Nematic insulator state at  $(\mu = -1, A = 0.14)$ ; (d) QSHI state at  $(\mu = -1, A = 0.15)$ .

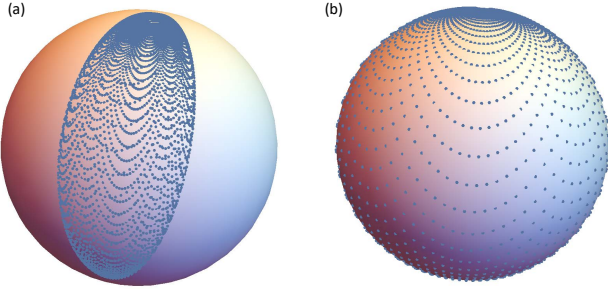


FIG. 6: (Color online) Plots of Bloch spheres. (a) Nematic insulator state at  $(\mu = -1, A = 0.14)$ ; (b) QSHI state at  $(\mu = -1, A = 0.15)$ .

by  $\Delta_{\vec{k}}$  vortices that are located away from  $\vec{k} = 0$  and outside the zero-line when one is present, as illustrated in Fig. 5(a) and (c). The normal insulator and QSHI states both have  $\Delta_{\vec{k}}$  vortices at  $\vec{k} = 0$ , as illustrated in Fig. 5(b) and (d), but a zero line is present only for the QSHI state in Fig. 5(d).

States with vortices away from  $\vec{k} = 0$ , but inside the zero-line, which would be nematic topological insulator states, did not appear in our mean-field calculations. Instead, as  $A$  increases from a point inside the nematic insulator region the ground state vortex position always

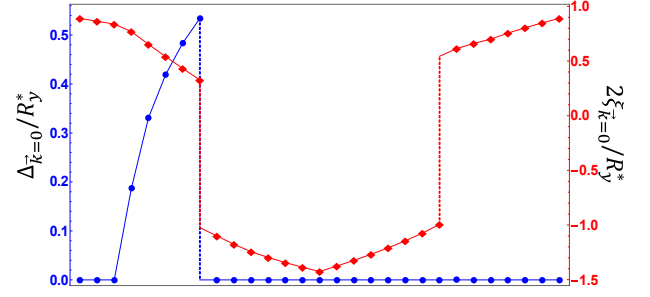


FIG. 7: (Color online) Plots of  $\Delta_{\vec{k}=0}$  and  $2\xi_{\vec{k}=0}$  at different parameter space. Blue dot denotes off-diagonal terms at origin, and only nematic insulator phase has non-zero value. Red square denotes diagonal difference terms at origin, and phase transitions of both nematic insulator/QSHI and NI/QSHI are first order. Phase transition between nematic to normal insulator is second order.

jumps discontinuously from outside the zero line to the origin. This vortex position jump demonstrates that the nematic insulator to QSHI phase transition is first order. The critical value of  $A$  at which the transition occurs decreases when  $E_{gap}$  decreases because the zero-line becomes moves to larger momentum magnitude as the bare gap decreases.

In Fig. 6 we illustrate the relationship the connection between the vortex positions relative to zero-line and band Chern numbers by providing a Bloch sphere representation of the dependence of occupied quasiparticle state on momentum. We have mapped states on our momentum-space grid are mapped to the Bloch unit sphere  $(\sin(\theta_B) \cos(\phi_B), \sin(\theta_B) \sin(\phi_B), \cos(\theta_B))$  using  $\cos(\theta_B) = \xi_{\vec{k}}/E_{\vec{k}}$  and  $\cos \phi_B = -\frac{|\Delta_{\vec{k}}| \cos(\phi_{\vec{k}})}{E_{\vec{k}}}$ . In a topological nontrivial state, the mapping from momentum space covers the whole Bloch sphere, as illustrated in Fig. 6(b). A zero-line is necessary for points to cross the equator and only a vortex inside a zero-line can cover the entire equator.

We take a careful look at phase transition areas (a gray square) where three phase transition lines touch together as shown in Fig. 4. To determine whether the phase transitions between different phases are continuous or not, we plot order parameter  $\Delta_{\vec{k}=0}$  and renormalized gap  $2\xi_{\vec{k}=0}$  at various parameters along the gray square. In Fig. 7, blue dots represent nematic order parameters  $\Delta_{\vec{k}=0}$  and only nematic insulator phase has non-zero value. Red squares represent differences in diagonal terms at  $\vec{k} = 0$  and QSHI requires the renormalized gap

to be negative. Along the gray square, first phase transition normal insulator/nematic insulator is second order because both  $\Delta_{\vec{k}=0}$  and  $2\xi_{\vec{k}=0}$  changes continuously with discontinuous slope. Then second phase transition nematic insulator/QSHI is first order because of a discontinuous jump in both terms guided by dashed vertical lines. Third phase transition QSHI/normal insulator is also first order because of a discontinuous jump in renormalized gap. This is unexpected for a non-interacting topological phase transition where the gap between conduction and valence band closes continuously. But due to the long-range Coulomb interaction, even NI/QSHI phase transition at small band gap becomes first order. When band gap is very large, we expect the NI/QSHI transition to be continuous again as Coulomb interaction becomes irrelevant. This critical band gap value has been marked as red star in Fig. 4.

\* Electronic address: feixue@utexas.edu

† Electronic address: macd@physics.utexas.edu

- [1] C. L. Kane and E. J. Mele, Phys. Rev. Lett. **95**, 226801 (2005).
- [2] C. L. Kane and E. J. Mele, Phys. Rev. Lett. **95**, 146802 (2005).
- [3] B. A. Bernevig, T. L. Hughes, and S.-C. Zhang, Science **314**, 1757 (2006), <http://science.sciencemag.org/content/314/5806/1757.full.pdf>.
- [4] C. Liu, T. L. Hughes, X.-L. Qi, K. Wang, and S.-C. Zhang, Phys. Rev. Lett. **100**, 236601 (2008).
- [5] M. König, S. Wiedmann, C. Brüne, A. Roth, H. Buhmann, L. W. Molenkamp, X.-L. Qi, and S.-C. Zhang, Science **318**, 766 (2007), <http://science.sciencemag.org/content/318/5851/766.full.pdf>.
- [6] A. Kononov, S. V. Egorov, Z. D. Kvon, N. N. Mikhailov, S. A. Dvoretzky, and E. V. Deviatov, JETP Letters **101**, 814 (2015).
- [7] P. Leubner, L. Lunczer, C. Brüne, H. Buhmann, and L. W. Molenkamp, Phys. Rev. Lett. **117**, 086403 (2016).
- [8] E. Bocquillon, R. S. Deacon, J. Wiedenmann, P. Leubner, T. M. Klapwijk, C. Brüne, K. Ishibashi, H. Buhmann, and L. W. Molenkamp, Nat. Nanotechnol. **12**, 137 (2017).
- [9] K.-M. Dantscher, D. A. Kozlov, M. T. Scherr, S. Gebert, J. Bärenfänger, M. V. Durnev, S. A. Tarasenko, V. V. Bel'kov, N. N. Mikhailov, S. A. Dvoretzky, Z. D. Kvon, J. Ziegler, D. Weiss, and S. D. Ganichev, Phys. Rev. B **95**, 201103 (2017).
- [10] I. Knez, R.-R. Du, and G. Sullivan, Phys. Rev. Lett. **107**, 136603 (2011).
- [11] V. S. Pribiag, A. J. A. Beukman, F. Qu, M. C. Cassidy, C. Charpentier, W. Wegscheider, and L. P. Kouwenhoven, Nat. Nanotechnol. **10**, 593 (2015).
- [12] L. Du, X. Li, W.-K. Lou, G. Sullivan, K. Chang, J. Kono, and R.-R. Du, Nat. Commun. **8**, 1971 (2017).
- [13] L. Du, T. Li, W. Lou, X. Wu, X. Liu, Z. Han, C. Zhang, G. Sullivan, A. Ikhlassi, K. Chang, and R.-R. Du, Phys. Rev. Lett. **119**, 056803 (2017).
- [14] A. Kononov, V. A. Kostarev, B. R. Semyagin, V. V. Preobrazhenskii, M. A. Putyato, E. A. Emelyanov, and E. V. Deviatov, Phys. Rev. B **96**, 245304 (2017).
- [15] L. V. Keldysh and Y. V. Kopayev, Sov. Phys. Solid State **6**, 2219 (1965).
- [16] Y. E. Lozovik and V. I. Yudson, Sov. Phys. JETP **44**, 389 (1976).
- [17] C. Comte and P. Nozieres, J. Phys. (Paris) **43**, 1069 (1982).
- [18] C. Liu and S. Zhang, in *Topological Insulators*, Contemporary Concepts of Condensed Matter Science, Vol. 6, edited by M. Franz and L. Molenkamp (Elsevier, 2013) pp. 59 – 89.
- [19] W. Yu, V. Clericò, C. Hernández Fuentevilla, X. Shi, Y. Jiang, D. Saha, W. K. Lou, K. Chang, D. H. Huang, G. Gumbs, D. Smirnov, C. J. Stanton, Z. Jiang, V. Bellani, Y. Meziani, E. Diez, W. Pan, S. D. Hawkins, and J. F. Klem, ArXiv e-prints (2017), arXiv:1701.07417 [cond-mat.mtrl-sci].
- [20] J. C. Budich, B. Trauzettel, and P. Michetti, Phys. Rev. Lett. **112**, 146405 (2014).
- [21] D. I. Pikulin and T. Hyart, Phys. Rev. Lett. **112**, 176403 (2014).
- [22] X. Zhu, P. B. Littlewood, M. S. Hybertsen, and T. M. Rice, Phys. Rev. Lett. **74**, 1633 (1995).
- [23] Y. E. Lozovik and O. L. Berman, Journal of Experimental and Theoretical Physics Letters **64**, 573 (1996).
- [24] J. Fernández-Rossier, C. Tejedor, L. Muñoz, and L. Viña, Phys. Rev. B **54**, 11582 (1996).
- [25] L. Vina, J. Phys. Condens. Matter **11**, 5929 (1999).
- [26] M. Combescot, O. Betbeder-Matibet, and F. Dubin, Phys. Rep. **463**, 215 (2008).
- [27] M. Combescot and D. W. Snoke, Phys. Rev. B **78**, 144303 (2008).
- [28] A. A. High, J. R. Leonard, A. T. Hammack, M. M. Fogler, L. V. Butov, A. V. Kavokin, K. L. Campman, and A. C. Gossard, Nature(London) **483**, 584 (2012).
- [29] A. Perali, D. Neilson, and A. R. Hamilton, Phys. Rev. Lett. **110**, 146803 (2013).
- [30] F.-C. Wu, F. Xue, and A. H. MacDonald, Phys. Rev. B **92**, 165121 (2015).
- [31] X. Wu, R.-R. Du, W. Lou, T. Li, K. Chang, and G. Sullivan, manuscript in preparation.
- [32] A. Y. Vul', "GALLIUM ANTIMONIDE (GaSb)," in *Handbook Series on Semiconductor Parameters* (WORLD SCIENTIFIC, 2012) pp. 125–146.
- [33] M. P. Mikhailova, "INDIUM ARSENIDE (InAs)," in *Handbook Series on Semiconductor Parameters* (WORLD SCIENTIFIC, 2012) pp. 147–168.
- [34] B. Roy, P. Goswami, and J. D. Sau, Phys. Rev. B **94**, 041101 (2016).
- [35] A. H. MacDonald, J. Jung, and F. Zhang, Physica Scripta **2012**, 014012 (2012).
- [36] G. W. Semenoff, Physica Scripta **2012**, 014016 (2012).
- [37] A. Amaricci, J. C. Budich, M. Capone, B. Trauzettel, and G. Sangiovanni, Phys. Rev. Lett. **114**, 185701 (2015).
- [38] K. Jiang, S. Zhou, X. Dai, and Z. Wang, Phys. Rev. Lett. **120**, 157205 (2018).
- [39] R. Yu, X. L. Qi, A. Bernevig, Z. Fang, and X. Dai, Phys. Rev. B **84**, 075119 (2011).
- [40] H. Weng, R. Yu, X. Hu, X. Dai, and Z. Fang, Advances in Physics **64**, 227 (2015), <http://dx.doi.org/10.1080/00018732.2015.1068524>



- [41] L. Liu, L. Świerkowski, and D. Neilson, *Physica B* **249-251**, 594 (1998).
- [42] S. De Palo, F. Rapisarda, and G. Senatore, *Phys. Rev. Lett.* **88**, 206401 (2002).
- [43] V. V. Nikolaev and M. E. Portnoi, *Superlattices Microstruc.* **43**, 460 (2008).
- [44] K. Asano and T. Yoshioka, *J. Phys. Soc. Jpn.* **83**, 084702 (2014).
- [45] J.-J. Su and A. H. MacDonald, *Nature Phys.* **4**, 799 (2008).
- [46] K. Sun, H. Yao, E. Fradkin, and S. A. Kivelson, *Phys. Rev. Lett.* **103**, 046811 (2009).
- [47] A. M. Cook, C. Hickey, and A. Paramakanti, *Phys. Rev. B* **90**, 085145 (2014).
- [48] Z. Fei, T. Palomaki, S. Wu, W. Zhao, X. Cai, B. Sun, P. Nguyen, J. Finney, X. Xu, and D. H. Cobden, *Nat. Phys.* **13**, 677 (2017).
- [49] S. Tang, C. Zhang, D. Wong, Z. Pedramrazi, H.-Z. Tsai, C. Jia, B. Moritz, M. Claassen, H. Ryu, S. Kahn, J. Jiang, H. Yan, M. Hashimoto, D. Lu, R. G. Moore, C.-C. Hwang, C. Hwang, Z. Hussain, Y. Chen, M. M. Ugeda, Z. Liu, X. Xie, T. P. Devereaux, M. F. Crommie, S.-K. Mo, and Z.-X. Shen, *Nat. Phys.* **13**, 683 (2017).
- [50] S. Wu, V. Fatemi, Q. D. Gibson, K. Watanabe, T. Taniguchi, R. J. Cava, and P. Jarillo-Herrero, *Science* **359**, 76 (2018), <http://science.sciencemag.org/content/359/6371/76.full.pdf>
- [51] X. Qian, J. Liu, L. Fu, and J. Li, *Science* (2014), 10.1126/science.1256815, <http://science.sciencemag.org/content/early/2014/11/19/science.1256815>